ChemComm

COMMUNICATION

View Article Online
View Journal | View Issue

Cite this: *Chem. Commun.*, 2023, **59**, 1959

Received 1st December 2022,
Accepted 18th January 2023

DOI: 10.1039/d2cc06557f

rsc.li/chemcomm

Potentiometric nanosensor for real-time measurement of hydrogen sulfide in single cell†

Shuwen Cheng, Shuai Zhang, Rantong Liu, Hui Zeng, Yongyue Yin and Meining Zhang *

One potentiometric nanosensor for monitoring intracellular hydrogen sulfide (H_2S) with fast potential response, high selectivity and excellent antifouling properties was developed. This study constructs a powerful tool to real-time track the changes of intracellular H_2S *in situ*, promoting the future studies of physiologically relevant processes.

Hydrogen sulfide (H_2S), an important neuromodulator, is one of the three major gas signaling molecules.[1,2] Neurodegenerative diseases including Alzheimer's disease, Parkinson's disease and Huntington's disease are associated with the level of H_2S.[3–5] Endogenous H_2S plays an indispensable role *in vivo* by expanding blood vessels, regulating metabolism and resisting inflammation.[6–9] H_2S is involved in cellular regulatory processes including regulating intracellular pH, promoting calcium influx of neurons and facilitating *N*-methyl-D-aspartic acid (NMDA) receptors.[9] To the best of our knowledge, most of the sulfur stored in cells with different kinds of forms like acid-labile sulfur and bound sulfur, which will release H_2S under external stimulation.[10] Although chromatography,[11,12] fluorescence,[13–16] colorimetric assays[17–19] and electrochemical methods[19–21] have been used to detect H_2S in the brain or single cells, it is still challenging to real-time track intracellular H_2S *in situ* with fast response and selectivity.

Electrochemistry with high spatiotemporal resolution has been widely applied in monitoring neurochemicals released in biological and pathological systems continuously and rapidly.[22–25] To date, electrochemical sensing of H_2S can be realized through both amperometry and potentiometry. For example, Hu *et al.* developed a 3D porous structure to detect H_2S released from single HeLa cells with amperometric methods.[26] Dong *et al.* developed a biosensor for the monitoring of endogenous H_2S_n and H_2S with differential pulse voltammetry in hippocampal slices and living rats based on specific reaction.[27] However, the amperometric method faces the issue of contamination from sulfur in continuous measurement, resulting in low stability and sensitivity decrease. To address this problem, Pan *et al.* synthesized one single-atom catalyst for electrocatalytic H_2S at very low potential, which enables the construction of one stable H_2S sensor with galvanic redox potentiometry for real-time H_2S sensing in the living brain.[28] We developed one potential method to selectively track the dynamics of H_2S in the brain with Ag_2S coated Ag nanoparticles (AgNPs) on a microelectrode based on a potential method.[29] Compared to amperometric methods, potentiometry guided by the Nernst equation is independent of electrode area and has very small current flow, which will be beneficial for cell analysis. Therefore, we anticipate that our potentiometric sensor could be pushed to the nano-size and evaluate its feasibility in cell sensing.

Herein, we demonstrate one potentiometric method using a AgNP-modified carbon fiber nanoelectrode treated with Na_2S, forming Ag_2S/AgNPs/CFNE for the real-time monitoring of H_2S in a single cell with high selectivity and stability. We find that potentiometry is easily controlled for intracellular electrochemistry analysis comparing with amperometry. Moreover, Ag_2S/AgNPs/CFNE exhibits a highly selective and stable potential response to H_2S. Because Ag_2S/AgNPs/CFNE can resist acid and base interference, Ag_2S/AgNPs/CFNE is exploited as a powerful tool to achieve the continuous monitoring of H_2S in single cells with different pH environments. Beyond all that, we found that intracellular H_2S will be released upon the external stimulation of potassium. This real-time and *in situ* H_2S measurement method with high selectivity will present a new perspective in the study of physiology and pathophysiology associated with H_2S.

To demonstrate that the potential response is independent of electrode area, which is different from amperometric methods, cyclic voltammograms (CV) and the open-circuit potentials of the CFME and CFNE in HEPES buffer containing 1 mM $Ru(NH_3)_6^{3+}$ were compared (Fig. 1B and C). As shown in Fig. 1B, the current response of the CFME is 50 times larger than that of the CFNE. In contrast, both the CFME and CFNE have close

Department of Chemistry, Renmin University of China, Beijing, 100872, China. E-mail: mnzhang@ruc.edu.cn

† Electronic supplementary information (ESI) available: Experiment details, two tables and eleven figures. See DOI: https://doi.org/10.1039/d2cc06557f

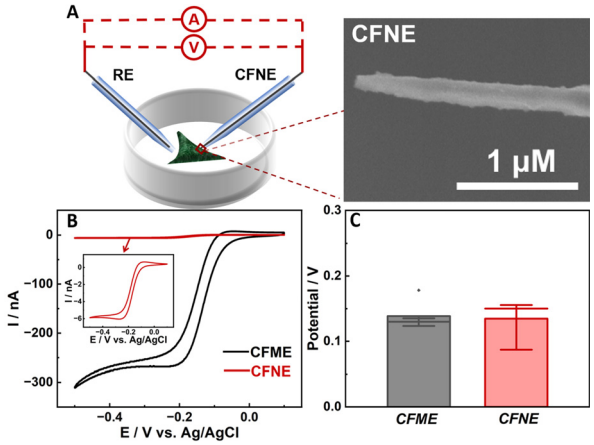

Fig. 1 (A) Scheme of the cell detection with the CFNE by using the amperometric method and open-circuit potential. Inset: SEM image of the bare CFNE. Cyclic voltammograms (B) and statistics potential response (C) obtained at the bare carbon fiber microelectrode (black) and carbon fiber nanoelectrode (red) in HEPES buffer containing 1 mM $Ru(NH_3)_6^{3+}$.

potential responses towards 1 mM $Ru(NH_3)_6^{3+}$ (*ca.* 150 mV) (Fig. 1C). For intracellular electrochemical analysis using the amperometric method, non-membrane permeable $Ru(NH_3)_6^{3+}$ is normally used to evaluate the insertion depth of the CFNE into the cell.[30] With the increase of the insertion depth of the CFNE into the cells incubated with HEPES buffer containing 1 mM $Ru(NH_3)_6^{3+}$, the reduction current decreased correspondingly. The OCP response did not change until the nanoelectrode inserted into the cell completely (Fig. S1, ESI†). These results indicate that open-circuit potential is easier to control for intracellular analysis because it is not necessary to ensure that the whole CFNE is inserted into the cell.

To develop one H_2S nanosensor, Ag nanoparticles (NPs) were electrodeposited on the CFNE building up a layer with a reversible redox equilibrium at the interface of AgNPs/CFNE. And the AgNPs/CFNE was further pre-treated with 5 μM Na_2S at open-circuit potential until the potential balanced for 300 s to form the Ag_2S/AgNPs/CFNE. The SEM image (Fig. 2A) and the corresponding energy dispersive spectrometer (EDS) elemental mapping (Fig. 2B and C) of the local Ag_2S/AgNPs/CFNE suggests the homogeneous decoration of Ag_2S/AgNPs on the surface of the CFNE.

To output OCP, Ag/AgCl was used as a reference electrode and the Ag_2S/AgNPs/CFNE as a working electrode. In this work, we mainly utilized Na_2S as the source of dissolved H_2S in the bulk electrolyte because there is a transformation between them in the solution:

$$H_2S \rightleftharpoons HS^- + H^+ \rightleftharpoons S^{2-} + 2H^+$$

Considering an insoluble salt electrode, the output potential OCP equals the potential difference between the indicated electrode and the reference electrode according to the Nernest equation, and the change of OCP response is only related to the concentration of S^{2-}:

$$\mathrm{OCP} = E^{\theta}_{\mathrm{Ag/Ag_2S}} - \frac{RT}{2F}\ln\left[S^{2-}\right] - E_R$$

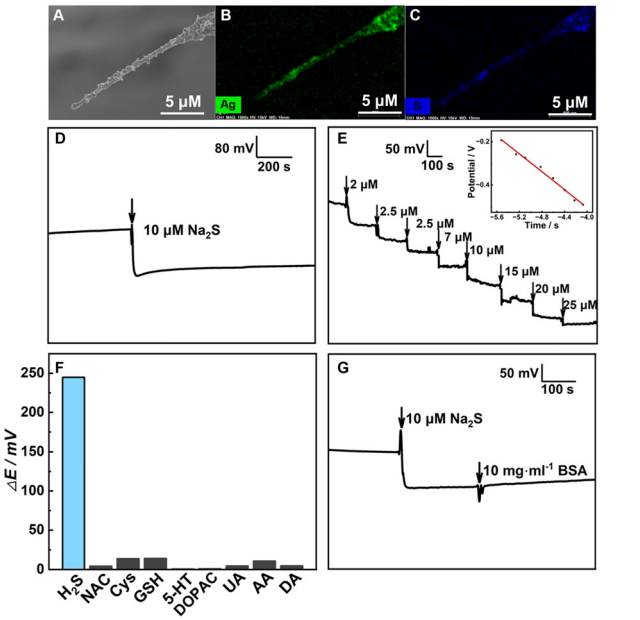

Fig. 2 (A) SEM image of the Ag_2S/AgNPs/CFNE. The elemental mapping images of (B) Ag and (C) S of the Ag_2S/AgNPs/CFNE. (D) The OCP response of the Ag_2S/AgNPs/CFNE towards 10 μM Na_2S for 1000 s in HEPES (pH = 7.4). (E) Typical OCP responses obtained at the Ag_2S/AgNPs/CFNE towards successive addition of Na_2S in HEPES (pH = 7.4) and the calibration plot of steady-state OCP output with the logarithmic concentration of H_2S. (F) Selective test of OCP response recorded at the Ag_2S/AgNPs/CFNE toward 20 μM DA, 200 μM AA, 50 μM UA, 20 μM DOPAC, 10 μM 5-HT, 200 μM GSH, 20 μM Cys, 20 μM NAC and 20 μM Na_2S in HEPES (pH = 7.4). (G) OCP signal obtained at the Ag_2S/Ag NPs/CFNE upon the addition of 10 μM Na_2S and 10 mg mL^{-1} BSA in HEPES (pH = 7.4) as labeled in the figure.

where $E^{\theta}_{\mathrm{Ag/Ag_2S}}$, R, T and F are the formal potential of Ag/Ag_2S, the universal gas constant, the temperature, and the Faraday constant, respectively. As we can see from Fig. 2D, the Ag_2S/AgNPs/CFNE exhibited an excellent steep potential response for 10 μM Na_2S in HEPES (pH = 7.4) and remained stable for 1000 s. The good stability is ascribed to there being no current flow in the OCP, resulting in no sulfur formation, which is ensured by no sulfur characteristic peak in the X-Ray photoelectron spectra of the electrode after detection (Fig. S2, ESI†). This nanoelectrode also exhibited a linear relationship (Fig. 2E) between the potential decrease and the logarithmic concentration gradient of H_2S from 2 μM to 84 μM (OCP (mV) = $-205.32\lg[S^{2-}]$ (μM) − 1324.14 (mV), R^2 = 0.9903). The detection limit for the nanoelectrode was estimated to be *ca.* 0.6 μM (S/N = 3). We also investigated the interference from the electroactive species and sulfur-containing species coexisting in the cell. The potential response of 20 μM dopamine (DA), 200 μM ascorbic acid (AA), 50 μM uric acid (UA), 20 μM dihydroxy-phenyl acetic acid (DOPAC), 10 μM 5-hydroxytryptamine (5-HT), 200 μM glutathione (GSH), 20 μM cysteine (Cys), and 20 μM *N*-acetyl-L-cysteine (NAC) shows a negligible response compared with that of 20 μM Na_2S at the Ag_2S/AgNPs/CFNE in HEPES buffer (Fig. 2F). These results indicate that Ag_2S/AgNPs/CFNE possesses good selectivity towards H_2S against these interferents. Furthermore, with the addition of bull serum albumin

(BSA) (10 mg mL^{-1}), the output potential (Fig. 2G) did not evidently change and was retained well resulting from the effective layer of Ag_2S/AgNPs and the inherent property of potentiometry. In summary, the properties of fast response, good stability, and high selectivity make the Ag_2S/AgNPs/CFNE greatly promising for real-time detection of H_2S.

Therefore, we applied this nanoelectrode to detect intercellular H_2S. As shown in Fig. 3A, the OCP response of the Ag_2S/AgNPs/CFNE presents an obvious decrease for about 18 mV after penetrating into one SH-SY5Y cell immediately, which is calculated to be 1.21 μM H_2S according to the calibration. In order to ensure the accuracy of this result, we investigated seven cells under the same experimental conditions and the same step, thus achieving the change of potential statistics for 16.32 ± 1.95 mV, with the corresponding intracellular H_2S being 1.20 ± 0.03 μM (Fig. 3B). Fig. 3C shows an image of a cell after inserting the Ag_2S/AgNPs/CFNE. The morphology of the cell didn't change dramatically after penetration by the Ag_2S/AgNPs/CFNE. The penetrated cells were stained by fluorescent Calcein-AM (green, live cell, Fig. 3D) and propidium iodide (PI) (red, dead cell, Fig. 3E) indicating negligible damage to the cells by the Ag_2S/AgNPs/CFNE. These results demonstrate that the Ag_2S/AgNPs/CFNE can measure the intracellular H_2S without affecting the cell activity.

H_2S in mammalian cells is produced by both enzymatic and nonenzymatic pathways, with the nonenzymatic pathway accounting for only a small fraction of synthesis. As studied previously, among the enzymatic pathways, two pyridoxal-5′-phosphate (PLP)-dependent enzymes including cystathionine β-synthase (CBS) and cystathionine γ-lyase (CSE), can catalyse Cys to produce H_2S. Cys is abundant in nerve cells and can be transformed from NAC.[31] In addition, a large amount of H_2S exists in different kinds of compounds in the cell. The critical pH value is one of the most essential factors impacting the release of stored sulfur in cells. Acid-labile released H_2S in acid conditions below pH 5.4 and bound sulfur released H_2S in alkaline conditions above pH 8.4 have been reported in previous articles.[10] First of all, we investigated whether the physiological concentration of NAC and the fluctuation of the pH would have interference, thus affecting the nanosensor selectivity. The result is shown in Fig. 4A and B. Compared with the evident potential decrease in the response to Na_2S, the output potential did not change evidently toward 1 mM NAC and with the change of pH by adding HCl and NaOH from 5.0 to 9.0. These results indicate that the Ag_2S/AgNPs/CFNE is stable enough to be suitable for tracking H_2S under the stimulation of NAC, acid and alkaline solutions. To further explore the physiologic stimuli that might enhance the stored sulfur to transform into free H_2S, we measured the change of OCP by the

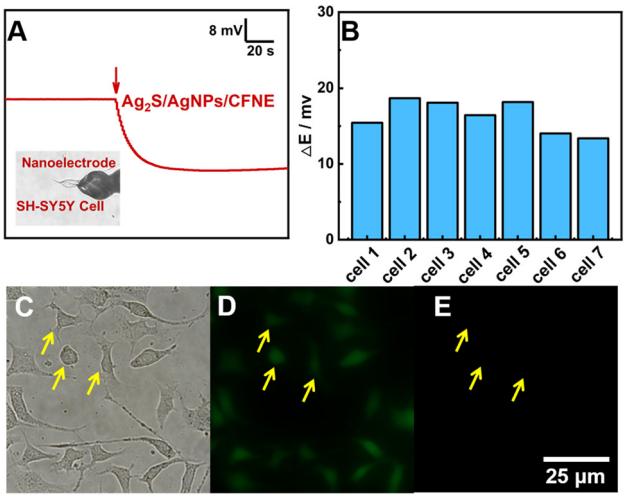

Fig. 3 (A) OCP response recorded by the Ag_2S/AgNPs/CFNE inserted into a SH-SY5Y cell. Inset is a bright-field image of a SH-SY5Y cell penetrated by the Ag_2S/AgNPs/CFNE. (B) The OCP responses for measurement of endogenous H_2S under the same conditions as in A. Bright-field image (C) and fluorescence image of SH-SY5Y cells stained with Calcein-AM (green, D) and PI (red, E) after penetration by the Ag_2S/AgNPs/CFNE for about 100 s indicated by yellow arrows.

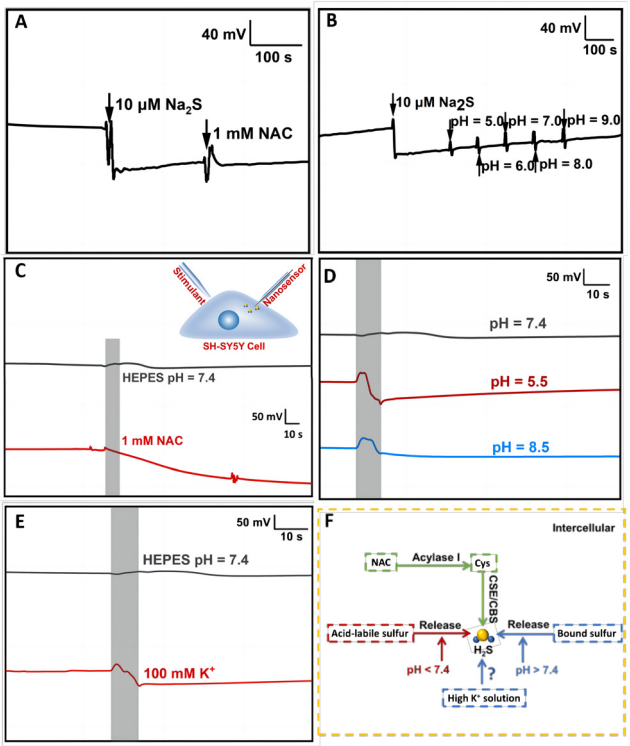

Fig. 4 (A) Typical OCP response recorded with the Ag_2S/AgNPs/CFNE toward 20 μM Na_2S and 1 mM NAC in HEPES (pH = 7.4). (B) Typical OCP response recorded with the Ag_2S/AgNPs/CFNE toward 20 μM Na_2S in HEPES (pH = 7.4) adjusting the pH value from 5.0 to 9.0 by adding HCl and NaOH as labeled in the figure. (C) Typical OCP response of the Ag_2S/AgNPs/CFNE in a single cell (n = 6) incubated with HEPES (pH = 7.4) stimulated with 1 mM NAC (red curve) and HEPES (pH = 7.4, grey curve). Inset is the illustration of the experimental setup for detecting H_2S using the nanosensor upon stimulation. (D) Typical OCP response of the Ag_2S/AgNPs/CFNE in a single cell (n = 6) incubated with HEPES (pH = 7.4) stimulated with HEPES with pH = 7.4 (grey curve), pH = 5.5 (red curve) and pH = 8.5 (blue curve). (E) Typical OCP response of the Ag_2S/AgNPs/CFNE in a single cell (n = 6) stimulated with HEPES (pH = 7.4, grey curve) and 100 mM K^+ solution (red curve). (F) Illustration of the synthetic and release pathway in the cell.

Ag_2S/AgNPs/CFNE inserted in a cell and stimulated by 1 mM NAC (2 μL s^{-1}, for 10 s) after the nanoelectrode achieved stability. As shown in Fig. 4C (red curve), after the addition of 1 mM NAC, the potential decreased slowly. In contrast, the addition of HEPES (pH = 7.4, grey curve) did not cause the decrease of the OCP. These results indicate that NAC has a positive influence on promoting the cell to release H_2S, which is consistent with reported literature,[30] suggesting that the Ag_2S/AgNPs/CFNE can monitor the release of H_2S. To illustrate the effects of different pH values on the release of H_2S, the solution (pH = 5.5, pH = 7.4 and pH = 8.5) was used to simulate the cell. The solution of pH 5.5 (Fig. 4D, red curve) and pH 8.5 (Fig. 4D, blue curve) leads to a quick OCP decrease. In contrast, injecting HEPES (pH = 7.4) as the control group, the output OCP potential response remained constant in the same time scale (Fig. 4D, grey curve). All these results demonstrate that the stored sulfur in cells will be released quickly in a short time when the pH value of the surroundings dramatically changes.

When neurons are excited, Na^+ enters and K^+ exits from cells, resulting in high K^+ concentrations in the extracellular environment and the depolarization of surrounding cells.[10] Inspired by this phenomenon, we applied this nanoelectrode to investigate whether stimulation with neuronal excitation (*i.e.* high concentration of K^+) will cause the release of H_2S. We found that an apparent potential decrease (Fig. 4E, red curve) was recorded after injecting 100 mM K^+ compared to that with HEPES at pH = 7.4 (Fig. 4E, grey curve). This result demonstrates that high K^+ concentrations can stimulate a fast release of H_2S. This release might result from the activation of the Na^+/HCO_3^- transporter by high K^+ concentration. However, the exact mechanism still needs to be studied further. Taken together, the overall results indicate that the Ag_2S/AgNPs/CFNE has the strong capability to real-time monitor H_2S release under different kinds of pathways (Fig. 4F) in living single cells with a quick response.

In summary, we have fabricated an Ag_2S/AgNPs/CFNE with high selectivity and stability for detecting H_2S continuously. The combined characteristics of the Ag_2S/AgNPs/CFNE with tiny dimensions, fast response and high sensitivity enable this nanoelectrode to real-time and *in situ* monitor the changes of endogenous H_2S in a single-cell under different conditions. We believe that this functional nanoelectrode will open up a new window for the understanding of H_2S in physiological and pathological processes.

We greatly acknowledge the financial support from the National Natural Science Foundation of China (Grant No. 21874152, 22174162).

Conflicts of interest

There are no conflicts to declare.

Notes and references

1 G. Yang, L. Wu, B. Jiang, W. Yang, J. Qi, K. Cao, Q. Meng, A. Mustafa, W. Mu, S. Zhang, S. Snyder and R. Wang, *Science*, 2008, **322**, 587–590.
2 H. Kimura, *Neurochem. Int.*, 2013, **63**, 492–497.
3 M. Wang, J. Tang, L. Wang, J. Yu, L. Zhang and C. Qiao, *Neural Regener. Res.*, 2021, **16**, 1353–1358.
4 J. Zhang, H. Shan, L. Tao and M. Zhang, *J. Mol. Neurosci.*, 2020, **70**, 2020–2030.
5 A. Ramya, M. Joseph, V. Karunakaran, C. Ahammed, A. Samanta and K. K. Maiti, *Sens. Actuators, B*, 2022, **355**, 131118.
6 C. Xu, F. Wu, P. Yu and L. Mao, *ACS Sens.*, 2019, **4**, 3102–3118.
7 H. Kimura, *Amino Acids*, 2011, **41**, 113–121.
8 Y. Wang, J. Li, Y. Qin, Q. Liu, Z. Liao and X. Xiao, *Exp. Clin. Endocrinol. Diabetes*, 2020, **128**, 137–143.
9 J. Wallace and R. Wang, *Nat. Rev. Drug Discovery*, 2015, **14**, 329–345.
10 M. Ishigami, K. Hiraki, K. Umemura, Y. Ogasawara, K. Ishii and H. Kimura, *Antioxid. Redox Signaling*, 2009, **11**, 205–214.
11 S. Koike, K. Kawamura, Y. Kimura, N. Shibuya, H. Kimura and Y. Ogasawara, *Free Radical Biol. Med.*, 2017, **113**, 355–362.
12 C. Hine, Y. Zhu, A. Hollenberg and J. Mitchell, *Antioxid. Redox Signaling*, 2018, **28**, 1483–1502.
13 S. Chen, Z. Chen, W. Ren and H. Ai, *J. Am. Chem. Soc.*, 2012, **134**, 9589–9592.
14 A. Lippert, E. New and C. Chang, *J. Am. Chem. Soc.*, 2011, **133**, 10078–10080.
15 Q. Zhong, R. Zhang, B. Yang, T. Tian, K. Zhang and B. Liu, *ACS Sens.*, 2022, **7**, 893–899.
16 L. Yan, Q. Gu, W. Jiang, M. Tan, Z. Tan, G. Mao, F. Xu and C. Li, *Anal. Chem.*, 2022, **94**, 5514–5520.
17 Z. Chen, C. Chen, H. Huang, F. Luo, L. Guo, L. Zhang, Z. Lin and G. Chen, *Anal. Chem.*, 2018, **90**, 6222–6228.
18 P. Zhang, Y. Hong, H. Wang, M. Yu, Y. Gao, R. Zeng, Y. Long and J. Chen, *Polym. Chem.*, 2017, **8**, 7271–7278.
19 C. Wang, M. Wang, W. Zhang, J. Liu, M. Lu, K. Li and Y. Lin, *Anal. Chem.*, 2020, **92**, 662–667.
20 T. Xu, N. Scafa, L. Xu, S. Zhou, K. Abdullah Al-Ghanem, S. Mahboob, B. Fugetsu and X. Zhang, *Analyst*, 2016, **141**, 1185–1195.
21 Y. Zhao, Y. Yang, L. Cui, F. Zheng and Q. Song, *Biosens. Bioelectron.*, 2018, **117**, 53–59.
22 M. Aref, E. Ranjbari, J. García-Guzmán, K. Hu, A. Lork, G. Crespo, A. Ewing and M. Cuartero, *Anal. Chem.*, 2021, **93**, 15744–15751.
23 X. Zhang, A. Hatamie and A. Ewing, *Curr. Opin. Electrochem.*, 2020, **22**, 94–101.
24 Y. Qi, H. Jiang, W. Wu, F. Zhang, S. Tian, W. Fan, Y. Liu, C. Amatore and W. Huang, *J. Am. Chem. Soc.*, 2022, **144**, 9723–9733.
25 R. Pan, D. Wang, K. Liu, H. Chen and D. Jiang, *J. Am. Chem. Soc.*, 2022, **144**, 17558–17566.
26 X. Hu, Y. Liu, H. Zhang, C. Xiao, Y. Qin, H. Duo, J. Xu, S. Guo, D. Pang and W. Huang, *ChemElectroChem*, 2016, **3**, 1998–2002.
27 H. Dong, Q. Zhou, L. Zhang and Y. Tian, *Angew. Chem., Int. Ed.*, 2019, **58**, 13948–13953.
28 C. Pan, F. Wu, J. Mao, W. Wu, G. Zhao, W. Ji, W. Ma, P. Yu and L. Mao, *J. Am. Chem. Soc.*, 2022, **144**, 14678–14686.
29 L. Zhang, T. Xu, W. Ji, X. Wang, S. Cheng, S. Zhang, Y. Zhang and M. Zhang, *Anal. Chem.*, 2021, **93**, 7063–7070.
30 W. Wu, X. Chen, Y. Jiao, W. Fan, Y. Liu and W. Huang, *Angew. Chem., Int. Ed.*, 2022, **61**, e202115820.
31 D. Ezerina, Y. Takano, K. Hanaoka, Y. Urano and T. Dick, *Cell Chem. Biol.*, 2018, **25**, 447–459.

